Shape resonances in the elastic scattering of slow electrons by pyridine

Alessandra S. Barbosa, Diego F. Pastega, and Márcio H. F. Bettega*

Departamento de Física, Universidade Federal do Paraná, Caixa Postal 19044, 81531-990, Curitiba, Paraná, Brazil

(Received 22 May 2013; revised manuscript received 2 July 2013; published 14 August 2013)

We present cross sections for elastic scattering of low-energy electrons with the N-heterocyclic molecule pyridine. We employed the Schwinger multichannel method implemented with pseudopotentials in the static-exchange and static-exchange-polarization approximations, for energies ranging from 0.1 to 12 eV. The calculated integral cross section presents two low-lying shape resonances of π^* nature belonging to the B_1 and A_2 symmetries and a higher lying resonance, belonging to the B_1 symmetry, which is a mixture of shape and core-excited resonances. The computed resonance positions are in reasonable agreement with the vertical attachment energy data of Nenner and Schulz [J. Chem. Phys. **62**, 1747 (1975)] and Modelli and Burrow [J. Electron Spectrosc. Relat. Phenom. **32**, 263 (1983)]. We compare the present calculated differential cross sections with the experimental data for benzene, pyrimidine, and pyridazine.

DOI: 10.1103/PhysRevA.88.022705 PACS number(s): 34.80.Bm, 34.80.Gs

I. INTRODUCTION

Nenner and Schulz [1], in the middle 1970′s, employed the electron transmission spectroscopy (ETS) technique to investigate the formation of temporary negative ions (TNIs) (shape resonances) in the electron interactions with benzene, pyridine, diazines (pyrazine, pyrimidine, and pyridazine), and s-triazine. For pyridine and diazines, they observed two low-lying π^* shape resonances and a third higher lying π^* resonance. They suspected that the third resonance was a shape resonance mixed with a core-excited resonance associated with low-lying excited states of the molecule. This suspicion has been confirmed recently by Winstead and McKoy [2,3] through calculations of electron collisions with pyrazine. Modelli and Burrow [4] also employed ETS to investigate TNI formation in electron interactions with pyridine and several substituted pyridines. In particular, they reported for pyridine three π^* resonances located at 0.72, 1.18, and 5.58 eV. By performing electronic structure calculations the authors assigned the resonances to the B_1, A_2, and B_1 symmetries, respectively. Recently, several theoretical and experimental studies have been performed on electron collisions with the diazines, in particular pyrimidine [5–12], most of them focusing on the shape resonances.

In this work we consider collisions of low-energy electrons with pyridine. This is an interesting molecule since it is obtained from benzene, which belongs to the D_{6h} group, by replacing a CH group by a nitrogen atom, resulting in a molecule with C_{2v} symmetry. Nenner and Schulz [1] reported three π^* resonances for pyridine located at 0.62, 1.20, and 4.58 eV which were assigned to the B_1, A_2, and B_1 symmetries, respectively. For the benzene molecule, the lowest resonance belongs to the E_{2u} symmetry and is located at 1.14 eV, being two-fold degenerate. As discussed by Nenner and Schulz [1], this resonance splits into two π^* resonances belonging to the B_1 and A_2 symmetries in pyridine, where the first (B_1) is at a lower energy than the E_{2u} resonance in benzene, and the second (A_2) is close to the first resonance in benzene.

Our purpose in the present study is to compute the cross sections for elastic scattering of electrons with pyridine and to identify the resonance spectrum. However, since the third resonance is a mixture of a shape resonance and a core-excited resonance, the inclusion of polarization effects demands extra care. In their study of collisions of low-energy electrons with pyrazine, Winstead and McKoy [2,3] have shown through a single-configuration interaction calculation of the negative ion that the third resonance of pyrazine, belonging to the B_{2g} symmetry, is associated with two main configurations, one from a shape resonance [the ground-state configuration of the target with the incoming electron occupying a $\pi^*(b_{2g})$ empty orbital] and the other from a core-excited resonance (associated to the low-lying triplet excited states of the target). Winstead and McKoy [2,3] have also shown that to obtain a correct location of the third (mixed) resonance, the $(N+1)$-particle basis set employed in the description of the polarization effects should be built from singlet- and triplet-coupled single excitations of the target.

Here we present elastic integral, momentum transfer and differential cross sections for electron collisions with pyridine. We employed the Schwinger multichannel method (SMC) [13] with pseudopotentials [14] in the static-exchange (SE) and in the static-exchange-polarization (SEP) approximations for energies ranging from 0.1 to 12 eV. We discuss different schemes to compute the polarization effects avoiding overcorrelation of the resonances. This is important since the lower and the higher resonances in pyridine belong to the same symmetry (B_1). In pyrazine each resonance belongs to different symmetries, and in pyrimidine the lower resonance belongs to the A_2 symmetry and the second and third resonances belong to the B_1 symmetry.

The remainder of this paper is organized as follows. In Sec. II we present the theoretical method and the computational procedures used in our calculations. In Sec. III we present and discuss our results. We close the paper with a brief summary of the present calculations and results in Sec. IV.

II. THEORY

To compute the elastic cross sections we employed the Schwinger multichannel method (SMC) [13] implemented

*bettega@fisica.ufpr.br

with pseudopotentials [14] within the minimal orbital basis for single-configuration interaction (MOB-SCI) approximation [15]. This method has been described in detail in several publications and here we will only discuss the points that are relevant to the present study.

The SMC method is a variational approximation of the scattering amplitude. The resulting expression in the body frame of the target is given by

$$f_{\mathrm{SMC}}(\vec{k}_f,\vec{k}_i) = -\frac{1}{2\pi}\sum_{m,n}\left\langle S_{\vec{k}_f}\middle|V|\chi_m\right\rangle (d^{-1})_{mn}\langle\chi_n|V\middle|S_{\vec{k}_i}\right\rangle, \quad (1)$$

where $\{|\chi_m\rangle\}$ represents a basis set of $(N+1)$-electron symmetry-adapted Slater determinants, also referred to as configuration state functions (CSFs). The CSFs are built from products of target states with single-particle functions. The d_{mn} matrix elements are given by

$$d_{mn} = \langle\chi_m|A^{(+)}|\chi_n\rangle, \quad (2)$$

and the $A^{(+)}$ operator is given by

$$A^{(+)} = \frac{1}{2}(PV+VP) - VG_P^{(+)}V + \frac{\hat{H}}{N+1} - \frac{1}{2}(\hat{H}P + P\hat{H}). \quad (3)$$

In the above equations $S_{\vec{k}_{i(f)}}$ is a product of a target state and a plane wave with momentum $\vec{k}_{i(f)}$, which is an eigenstate of the unperturbed Hamiltonian H_0; V is the interaction potential between the incident electron and the target; $\hat{H} = E - H$ is the total collision energy minus the full Hamiltonian of the system, where $H = H_0 + V$; P is a projection operator onto the open-channel space; and $G_P^{(+)}$ is the free-particle Green's function projected on the P space. In this work $P = |\Phi_1\rangle\langle\Phi_1|$, since we are considering only the elastic channel as open.

For the calculations performed in the SE approximation, the $(N+1)$-electron basis set (direct space) is given by

$$|\chi_m\rangle = \mathcal{A}(|\Phi_1\rangle \otimes |\varphi_m\rangle), \quad (4)$$

where $|\Phi_1\rangle$ represents the target ground state, $|\varphi_m\rangle$ is a single-particle function, and $\mathcal{A}$ is the antisymmetrizer. For the calculations performed in the SEP approximation, the direct space is augmented by CSFs constructed as

$$|\chi_m\rangle = \mathcal{A}(|\Phi_r\rangle \otimes |\varphi_s\rangle), \quad (5)$$

where $|\Phi_r\rangle$ are N-electron states obtained by performing single excitations of the target from the occupied (hole) orbitals to a set of unoccupied (particle) orbitals. Here $|\varphi_s\rangle$ is also a single-particle function and $\mathcal{A}$ is the antisymmetrizer.

To obtain the equilibrium geometry for the ground state of pyridine, we carried out a geometry optimization calculation at the second-order Møller-Plesset (MP2) level of approximation, with the TZV++$(2d,1p)$ basis set using the package GAMESS [16]. In Fig. 1 we present the geometrical structure of pyridine. In the scattering calculations we used the pseudopotentials of Bachelet, Hamann, and Schlüter [18] to replace the $1s$ core electrons of the carbon and nitrogen atoms. The Cartesian Gaussian functions used in our calculations are shown in Table I and were generated according to [19]. We used the Dunning $4s/3s$ basis set [20] for the hydrogen atom augmented by a p-type function with exponent 0.75. All d-type orbitals were considered as five component to avoid numerical instabilities.

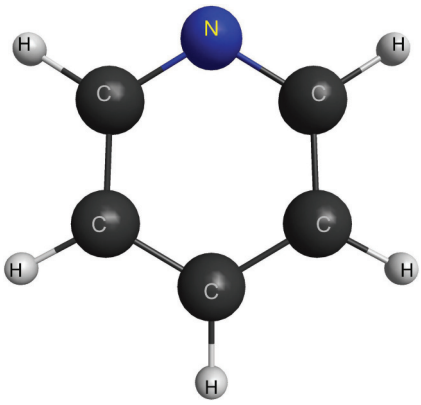

FIG. 1. (Color online) Geometrical structure of the pyridine molecule. Generated using MacMolPlt [17].

To represent the particle and the scattering orbitals in the SEP calculations we employed the improved virtual orbitals (IVOs) [21]. To construct the CSFs used in these calculations we employed a criteria [22] to select the hole, the particle, and the scattering orbitals given by

$$\varepsilon_{\mathrm{par}} - \varepsilon_{\mathrm{hole}} + \varepsilon_{\mathrm{scat}} < \Delta, \quad (6)$$

where $\varepsilon_{\mathrm{par}}$, $\varepsilon_{\mathrm{hole}}$, and $\varepsilon_{\mathrm{scat}}$ are the energies of the particle, hole, and scattering orbitals, respectively, and Δ is the energy cutoff. These criteria differ from the usual ones, which select the particle and the scattering orbitals up to a given energy $\varepsilon_{\mathrm{cutt}}$, by selecting these orbitals for each CSF individually. We used $\Delta = 1.895$ hartrees for all symmetries. For the nonresonant symmetries, namely, A_1 and B_2, we considered all singlet- and triplet-coupled excitations, and obtained 10 596 CSFs (doublets) for the A_1 symmetry and 10 470 CSFs for the B_2 symmetry.

In most cases, to take the polarization effects in the resonant symmetries into account, we consider only singlet-coupled excitations. This procedure helps to avoid overcorrelation, which brings the resonance to an energy below the experimental data (or even becoming a bound state) and was used for the A_2 and the B_1 symmetries. In this case we obtained 4697 CSFs

TABLE I. Uncontracted Cartesian Gaussian functions used for carbon and nitrogen in the calculation of pyridine.

Type	C	N
s	12.49408	17.569870
s	2.470291	3.423613
s	0.614027	0.884301
s	0.184029	0.259045
s	0.036799	0.053066
s	0.013682	0.022991
p	5.228869	7.050692
p	1.592058	1.910543
p	0.568612	0.579261
p	0.210326	0.165395
p	0.072250	0.037192
d	0.126278	0.208920

TABLE II. Excitation energies (in eV) for the five lowest excited states of pyridine.

State	E
$^3A_1$	3.482
$^3B_2$	4.672
$^3A_1$	5.004
$^1B_2$	6.116
$^1B_1$	6.123

for the B_1 symmetry and 4604 CSFs for the A_2 symmetry. However, as discussed by Nenner and Schluz [1] the third π^* resonance of pyridine is a mixture of shape and core-excited resonances, the latter being associated with the low-lying triplet excited states of the target. We present in Table II the excitation energies for the lowest five excited states of pyridine obtained in a single CI calculation using GAMESS [16] with a 6-311 + (d,p) basis set, with the geometry optimized at the MP2 level with the 6-31G(d) basis. Winstead and McKoy [2,3] showed that due to this mixed character, it is also necessary to include triplet-coupled excitations for a correct description of the position of the third resonance. Therefore we carried out two different calculations for the B_1 symmetry. In the first calculation we considered only singlet-coupled excitations, as described before, and in the second calculation we also included triplet-coupled excitations, totalizing 9272 CSFs for this symmetry.

The calculated dipole moment for pyridine is 2.470 D, which agrees relatively well with the experimental value of 2.215 D [23]. The SMC method employs only square integrable functions, more precisely Cartesian Gaussian (CG) functions, to represent the scattering wave function. In dealing with molecules that possess a permanent electric dipole moment, the long-range character of the dipole potential is truncated by the range of the CG functions, and therefore the higher partial waves are not properly described. To solve this problem, we included the dipole potential through a closure procedure [24]. We computed the scattering amplitude in the body frame of the molecular target and also computed the scattering amplitude for a point-dipole potential in the first Born approximation (FBA). We considered a dipole with the same orientation and magnitude as the molecular dipole used in the present SMC calculation. The final expression for the scattering amplitude is given by

$$f(\vec{k}_f,\vec{k}_i) = f^{\rm FBA}(\vec{k}_f,\vec{k}_i) + \sum_{\ell=0}^{\ell_{\rm SMC}} \sum_{m=-\ell}^{+\ell} \left[f_{\ell m}^{\rm SMC}(k_f,\vec{k}_i) - f_{\ell m}^{\rm FBA}(k_f,\vec{k}_i) \right] Y_{\ell m}^*(\hat{k}_f), \quad (7)$$

where $f_{\ell m}^{\rm SMC}$ and $f_{\ell m}^{\rm FBA}$ are obtained by expanding the angular dependence of the outgoing wave vector $\vec{k}_f$ of the SMC and the dipole FBA scattering amplitudes in partial waves. As a result, the lower partial waves of the scattering amplitude (up to $\ell = \ell_{\rm SMC}$) are considered from the SMC method, and the higher partial waves ($\ell > \ell_{\rm SMC}$) are considered from the first Born approximation for the dipole moment potential of the molecule. The divergence of the scattering amplitude at $\theta = 0^\circ$ is avoided according to the rotational spectrum of the target molecule by making $k_f^2 = k_i^2 + \Delta E_{\rm rot}$, where $\Delta E_{\rm rot} = 1.225 \times 10^{-5}$ eV obtained at the optimized geometry. The value of $\ell_{\rm SMC}$ depends on the energy and is chosen in order to provide the DCSs obtained with and without the Born closure correction in agreement at high scattering angles. We chose $\ell_{\rm SMC} = 1$ from 0.1 to 0.8 eV, $\ell_{\rm SMC} = 3$ from 0.9 to 2.9 eV, $\ell_{\rm SMC} = 4$ from 3 to 4.9 eV, $\ell_{\rm SMC} = 5$ from 5 to 6.9 eV, and $\ell_{\rm SMC} = 6$ from 7 to 12 eV.

III. RESULTS AND DISCUSSION

In Fig. 2 we present our calculated integral and momentum transfer cross sections for pyridine in the SE and SEP approximations for energies from 0.1 to 12 eV, where for the SEP approximation we present results with and without the Born closure. These SEP cross sections were obtained including singlet- and triplet-coupled excitations for A_1 and B_2 symmetries and singlet-coupled excitations for the B_1 and A_2 symmetries. There are two pronounced structures in these cross sections that represent the low-lying π_1^* and π_2^* resonances and another broader structure located at higher energies that corresponds to the π_3^* resonance. In the SEP cross sections, the structure corresponding to π_3^* overlaps with pseudoresonances. These pseudoresonances are associated with channels that are energetically accessible at these energies

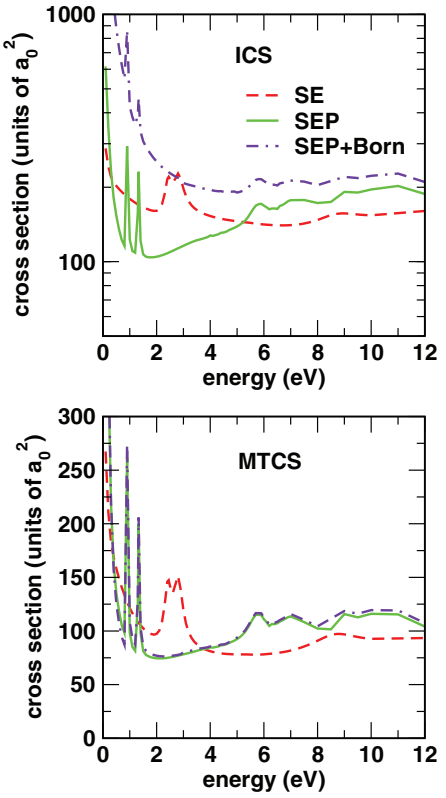

FIG. 2. (Color online) Integral (upper panel) and momentum transfer (lower panel) cross sections for elastic scattering of electrons by pyridine. The SEP cross sections were obtained by including singlet- and triplet-coupled excitations for A_1 and B_2 symmetries and singlet-coupled excitations for the B_1 and A_2 symmetries. The Born closure is employed only for the SEP calculations. See text for discussion.

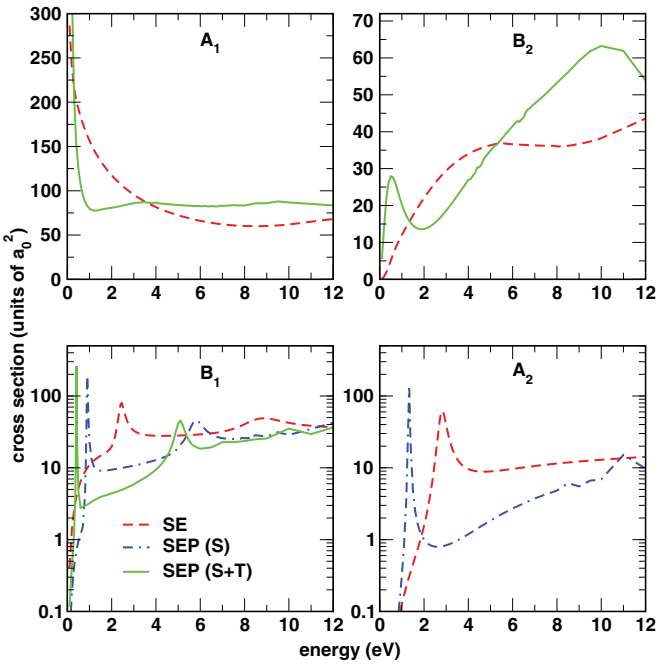

FIG. 3. (Color online) Symmetry decomposition of the integral cross section for elastic scattering of electrons by pyridine. See text for discussion.

but are treated as closed channels in the calculations. Opening those channels would soften the pseudoresonances [25]. The long-range character of the dipole interaction is responsible for the increase seen in the integral cross sections, while the position of the resonances are unaffected. This long-range interaction has little effect in the momentum transfer cross section.

Figure 3 shows the symmetry decomposition for the integral cross section of pyridine. This procedure allows one to assign the resonances seen in Fig. 2 to the symmetries of the C_{2v} group. This figure shows that π_1^* and π_3^* belong to the B_1 symmetry and π_2^* is assigned to the A_2 symmetry. In the SE cross sections, π_1^*, π_2^*, and π_3^* are located at 2.45, 2.8, and 8.9 eV, respectively. The inclusion of polarization effects moves π_2^* down in energy to 1.33 eV, in reasonable agreement with the ETS data of 1.20 eV reported by Nenner and Schulz [1] and of 1.18 eV reported by Modelli and Burrow [4].

As discussed before, π_3^* is a mixture of shape and core-excited resonances. As shown by Winstead and McKoy [2,3], to obtain the correct location of this resonance it is necessary to consider singlet- and triplet-coupled excitations in the description of the polarization effects. In Fig. 3 we present two sets of results for the B_1 symmetry corresponding to two different polarization calculations. In the first calculation we considered only singlet-coupled excitations, with π_3^* located at 5.80 eV, about 1.2–1.3 eV above the ETS values of 4.58 and 4.48 eV obtained by Nenner and Schulz [1] and by Modelli and Burrow [4], respectively. This calculation locates π_1^* at 0.90 eV, in reasonable agreement with the values of 0.62 eV obtained by Nenner and Schulz [1] and 0.72 eV obtained by Modelli and Burrow [4]. In the second calculation, we considered both singlet- and triplet-coupled excitations. In this case, π_3^* is located at 5.10 eV, in better agreement with the ETS

TABLE III. Resonance positions (in eV) for pyridine. We present the SEP results obtained considering only singlet-coupled excitations (S) and singlet- and triplet-coupled excitations (S + T). We also present the scaled VOEs. See text for discussion.

	π_1^* (B_1)	π_2^* (A_2)	π_3^* (B_1)
Present results (SE)	2.45	2.8	8.9
Present results (SEP - S)	0.90	1.33	5.80
Present results (SEP - S + T)	0.41		5.10
VOE_{MP2}	0.70	1.01	4.76
VOE_{B3LYP}	0.79	1.08	4.50
Nenner and Schulz [1]	0.62	1.20	4.58
Modelli and Burrow [4]	0.72	1.18	4.48

data. However, π_1^* lies below the experimental data, at around 0.41 eV. Although the position of π_3^* is improved with the inclusion of triplet-coupled excitations, π_1^* is overcorrelated. This was also observed by Palihawadana *et al.* [9] and by Ferraz *et al.* [12] in electron collisions with pyrimidine. The resonances obtained by Palihawadana [9] are in different order compared to the results of Nenner and Schulz [1] and Mašín *et al.* [6]. On the other hand, the lowest resonance of pyrimidine does not appear in the calculated cross sections of Ferraz *et al.* [12]. Our results are summarized in Table III.

To obtain further insight into the resonance spectrum of pyridine, we carried out additional electronic structure calculations using the program GAMESS [16]. We calculated the virtual orbital energies (VOEs), which can be related through Koopmans theorem to the vertical attachment energies (VAEs), and obtained plots for some unoccupied orbitals that represent an approximation to the resonant orbitals. We employed the empirical scaling relations from [26,27] and for the VOEs in two different calculations: (i) We optimized the ground-state geometry using second-order Møller-Plesset perturbation theory with the 6-31G(d), and we then carried out an energy calculation at the optimized geometry within the HF approximation with the same basis set. The calculated VOEs were scaled as VAE = 0.64795VOE − 1.4298 (the VAE and VOE are in eV). (ii) We performed geometry optimization and energy calculations based on the density functional theory (DFT) using the B3LYP functional and the 6-31G(d) basis set. The VOEs were scaled as VAE = 0.80543VOE + 1.21099 (the VAE and VOE are in eV). These results are also shown in Table III. Both calculations provide scaled VOEs in good agreement with the ETS data of Nenner and Schulz and Modelli and Burrow. We also obtained from the first calculation the lowest unoccupied molecular orbital (LUMO), the LUMO + 1, and the LUMO + 7, shown in Fig. 4. These π^* orbitals belong to the b_1, a_2, and b_1 symmetries and represent an approximation of the resonant orbitals. The DFT calculation provides LUMO, LUMO + 1, and LUMO + 4 as the resonant orbitals, with the same shape and symmetries as shown in Fig. 4.

Figure 5 shows the differential cross sections (DCSs) for pyridine at 2, 3, 4, 6, 8.5, and 10 eV, obtained in the SEP approximation with the Born closure. Also shown in this figure are the experimental DCSs for pyrimidine and pyrazine measured by Palihawadana *et al.* in two different studies [9,10] at 3, 6, and 10 eV, and for benzene measured by Cho *et al.* [28] at all energies above. In general the calculated DCSs for

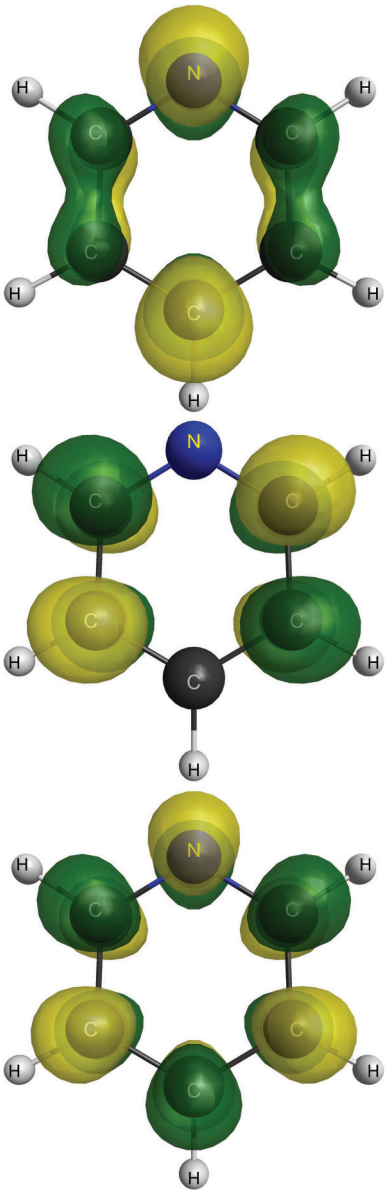

FIG. 4. (Color online) Top: LUMO, $\pi^*(b_1)$; middle: LUMO + 1, $\pi^*(a_2)$; bottom: LUMO + 7, $\pi^*(b_1)$. See text for discussion. Generated using MACMOLPLT [17].

pyridine and the experimental DCSs for pyrimidine, pyrazine, and benzene are very similar among themselves suggesting that the replacement of a CH group in benzene by one nitrogen in pyridine and by two nitrogen atoms in pyrazine and pyrimidine has little effect in the DCSs at these energies. Some differences are observed at lower scattering angles, where the DCSs of pyridine increase due to the permanent dipole moment of this molecule. At 6 eV the calculated DCS presents a shape quite different from the experimental data, and shows an f-wave behavior. This is the influence of the π_3^* resonance of pyridine, which is located at 5.8 eV in this calculation. At 10 eV, the calculated DCSs lies above the experimental data. This behavior may indicate that at this energy it would be important to allow flux loss from the elastic channel into the inelastic ones by opening the inelastic channels, lowering the elastic cross section towards the experiment [25].

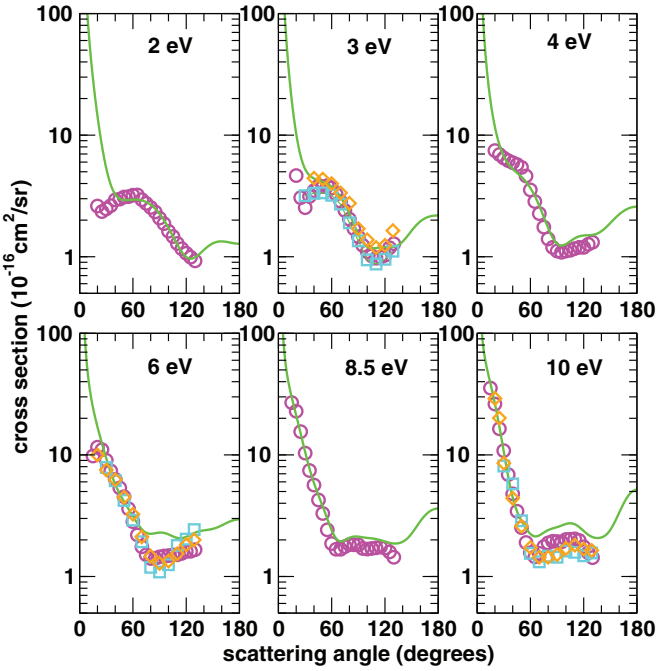

FIG. 5. (Color online) Differential cross sections for elastic electron collisions with pyridine at 2, 3, 4, 6, 8.5, and 10 eV. Solid (green) line: present results obtained in the SEP approximation including singlet- and triplet-coupled excitations for A_1 and B_2 symmetries and singlet-coupled excitations for the B_1 and A_2 symmetries. The Born closure was also employed in these calculations. Squares (cyan): experimental data for pyrimidine from [9]; diamonds (orange): experimental data for pyrazine from [10]; circles (magenta): experimental data for benzene from [28].

IV. CONCLUSIONS

We reported elastic integral, momentum transfer, and differential cross sections for collisions of low-energy electrons with pyridine. We found two low-lying resonances in the B_1 and A_2 symmetries and a higher lying resonance in the B_1 symmetry. We employed two different treatments of polarization to the B_1 symmetry in order to obtain a correct location of the third resonance, which is a mixture of shape and core-excited resonances. Our results are in reasonable agreement with the experimental data of Nenner and Schulz and Modelli and Burrow. We compared our calculated differential cross sections with the experimental data of Palihawadana *et al.* for pyrazine and pyrimidine and of Cho *et al.* for benzene. The calculated differential cross sections and the experimental data are very similar among themselves.

ACKNOWLEDGMENTS

A.S.B and D.F.P. acknowledge support from the Brazilian Agency Coordenação de Aperfeiçoamento de Pessoal de Nível Superior (CAPES). M.H.F.B. acknowledges support from the Brazilian agency Conselho Nacional de Desenvolvimento Científico e Tecnológico (CNPq), and from FINEP (under project CT-Infra). The authors acknowledge computational support from Professor Carlos M. de Carvalho at LFTC-DFis-UFPR and at LCPAD-UFPR, and from CENAPAD-SP.

[1] I. Nenner and G. J. Schulz, J. Chem. Phys. **62**, 1747 (1975).
[2] C. Winstead and V. McKoy, Phys. Rev. Lett. **98**, 113201 (2007).
[3] C. Winstead and V. McKoy, Phys. Rev. A **76**, 012712 (2007).
[4] A. Modelli and P. D. Burrow, J. Electron Spectrosc. Relat. Phenom. **32**, 263 (1983).
[5] Z. Mašín and J. D. Gorfinkiel, J. Chem. Phys. **135**, 144308 (2011).
[6] Z. Mašín, J. D. Gorfinkiel, D. B. Jones, S. M. Bellm, and M. J. Brunger, J. Chem. Phys. **136**, 144310 (2012).
[7] Z. Mašín and J. D. Gorfinkiel, J. Chem. Phys. **137**, 204312 (2012).
[8] A. Zecca, L. Chiari, G. García, F. Blanco, E. Trainotti, and M. J. Brunger, J. Phys. B **43**, 215204 (2010).
[9] P. Palihawadana, J. P. Sullivan, M. Brunger, C. Winstead, V. McKoy, G. Garcia, F. Blanco, and S. Buckman, Phys. Rev. A **84**, 062702 (2011).
[10] P. Palihawadana, J. P. Sullivan, S. J. Buckman, and M. J. Brunger, J. Chem. Phys. **137**, 204307 (2012).
[11] D. B. Jones, S. M. Bellm, P. Limão-Vieira, and M. J. Brunger, Chem. Phys. Lett. **535**, 30 (2012).
[12] J. R. Ferraz, A. S. dos Santos, G. L. C. de Souza, A. I. Zanelato, T. R. M. Alves, M.-T. Lee, L. M. Brescansin, R. R. Lucchese, and L. E. Machado, Phys. Rev. A **87**, 032717 (2013).
[13] K. Takatsuka and V. McKoy, Phys. Rev. A **24**, 2473 (1981); **30**, 1734 (1984).
[14] M. H. F. Bettega, L. G. Ferreira, and M. A. P. Lima, Phys. Rev. A **47**, 1111 (1993).
[15] R. F. da Costa, F. J. da Paixão, and M. A. P. Lima, J. Phys. B **37**, L129 (2004); **38**, 4363 (2005).
[16] M. W. Schmidt, K. K. Baldridge, J. A. Boatz, S. T. Elbert, M. S. Gordon, J. H. Jensen, S. Koseki, N. Matsunaga, K. A. Nguyen, S. J. Su, T. L. Windus, M. Dupuis, and J. A. Montgomery, J. Comput. Chem. **14**, 1347 (1993).
[17] B. M. Bode and M. S. Gordon, J. Mol. Graphics Mod. **16**, 133 (1998).
[18] G. B. Bachelet, D. R. Hamann, and M. Schlüter, Phys. Rev. B **26**, 4199 (1982).
[19] M. H. F. Bettega, A. P. P. Natalense, M. A. P. Lima, and L. G. Ferreira, Int. J. Quantum Chem. **60**, 821 (1996).
[20] T. H. Dunning, Jr., J. Chem. Phys. **53**, 2823 (1970).
[21] W. J. Hunt and W. A. Goddard, III, Chem. Phys. Lett. **3**, 414 (1969).
[22] F. Kossoski and M. H. F. Bettega, J. Chem. Phys. **138**, 234311 (2013).
[23] *CRC Handbook of Chemistry and Physics*, 79th ed., edited by D. R. Lide (CRC, Boca Raton, 1998).
[24] E. M. de Oliveira, R. F. da Costa, S. d'A. Sanchez, A. P. P. Natalense, M. H. F. Bettega, M. A. P. Lima, and M. T. do N. Varella, Phys. Chem. Chem. Phys. **15**, 1682 (2013).
[25] R. F. da Costa, M. H. F. Bettega, M. A. P. Lima, M. C. A. Lopes, L. R. Hargreaves, G. Serna, and M. A. Khakoo, Phys. Rev. A **85**, 062706 (2012).
[26] S. S. Staley and J. T. Strnad, J. Phys. Chem. **98**, 161 (1994).
[27] A. Modelli, Phys. Chem. Chem. Phys. **5**, 2923 (2003).
[28] H. Cho, R. J. Gulley, K. Sunohara, M. Kitajima, L. J. Uhlmann, H. Tanaka, and S. J. Buckman, J. Phys. B **34**, 1019 (2001).